OES Opto-Electronic Science

# Polygonal generalized perfect spatiotemporal optical vortices

Shuoshuo Zhang, Zhangyu Zhou, Qianyi Wei, Zhongsheng Man, Changjun Min, Wending Zhang, Yuquan Zhang*, Ting Mei* and Xiaocong Yuan

https://doi.org/10.29026/oes.2026.250041

Opto-Electronic Science

CN 51-1800/O4 ISSN (Print) 2097-0382 ISSN (Online) 2097-4000

# Polygonal generalized perfect spatiotemporal optical vortices

Shuoshuo Zhang, Zhangyu Zhou, Qianyi Wei, Zhongsheng Man, Changjun Min, Wending Zhang, Yuquan Zhang*, Ting Mei* and Xiaocong Yuan

**Citation:** Zhang SS, Zhou ZY, Wei QY et al. Polygonal generalized perfect spatiotemporal optical vortices. *Opto-Electron Sci* **5**, 250041 (2026).

https://doi.org/10.29026/oes.2026.250041

Received: 15 November 2025; Accepted: 6 March 2026; Published online: 25 March 2026

## Related articles

Opto-Electronic Science

Article

March 2026, Vol. 5, No. 3

Open Access

# Polygonal generalized perfect spatiotemporal optical vortices

Shuoshuo Zhang[1,2], Zhangyu Zhou[2], Qianyi Wei[2], Zhongsheng Man[3], Changjun Min[2], Wending Zhang[1], Yuquan Zhang[2]*, Ting Mei[1]* and Xiaocong Yuan[2]

**Abstract:** Recently, perfect spatiotemporal optical vortices (PSTOVs) have attracted significant attention due to their topological-charge-independent radius and their ability to carry transverse orbital angular momentum. However, existing studies on PSTOVs remain largely restricted to the simplest annular intensity profiles, limiting their versatility in tailoring light-matter interactions. Extending PSTOVs toward programmable distributions is therefore highly desirable for both fundamental studies and practical applications. To fill this research gap, we propose the concept of generalized perfect spatiotemporal optical vortices (GPSTOVs), whose intensity profiles can be flexibly engineered while preserving their intrinsic "perfect" properties. Unlike previous complex-amplitude modulation approaches, GPSTOV pulses are generated via a pure-phase modulation scheme, enabling higher modulation efficiency and improved energy utilization. By encoding a shape-controllable digital axicon and a vortex phase in the spatiotemporal frequency domain, we experimentally realize a family of polygonal GPSTOV pulses with tunable geometries. The measured spatiotemporal profiles agree well with theoretical predictions. Our results expand the scope of PSTOV research and hold promises for applications in optical communications, particle manipulation, and other fields requiring precise spatiotemporal control of ultrafast light pulses.

**Keywords:** spatiotemporally structured light; transverse orbital angular momentum; generalized perfect spatiotemporal optical vortices; pure-phase modulation

DOI: 10.29026/oes.2026.250041 | CSTR: 32246.14.oes.2026.250041

Citation: Zhang SS, Zhou ZY, Wei QY et al. Polygonal generalized perfect spatiotemporal optical vortices. *Opto-Electron Sci* **5**, 250041 (2026).

## 1 Introduction

Structured light can carry two types of angular momenta: spin angular momentum (SAM) and orbital angular momentum (OAM). SAM is related to the circular polarization of light, whereas OAM is commonly associated with the helical wavefronts of optical vortices[1]. In 1992, Allen et al. first demonstrated that Laguerre-Gaussian beams, characterized by a helical phase factor $\exp(i\ell\varphi)$, possess an intrinsic OAM of $\ell\hbar$ per photon ($\ell$ is the topological charge, $\varphi$ is the azimuthal angle, and $\hbar$ is the Dirac constant)[2]. Since then, significant progress has been made in the generation and manipulation of optical vortices[3–7]. Unlike SAM having only two possible values of $\pm\hbar$, the OAM of optical vortices can take theoretically unlimited values. Due to this prominent property, optical vortices can be applied a wide range of applications, including optical trapping[8,9], optical communications[10,11], super-resolution imaging[12], and quantum information processing[13,14], etc.

Optical vortices can be generated not only in the spatial domain but also in the spatiotemporal domain. Spatiotemporal optical vortices (STOVs) are structured pulsed beams that possess transverse OAM perpendicular to the propagation direction[15,16]. STOVs were first observed during the nonlinear self-focusing of femtosecond pulses[17], and were subsequently generated in a linear manner using a 4f pulse shaper[18]. Over the past few years, extensive studies have been devoted to STOVs, covering their generation[19–26], characterization[27–29], fundamental properties[30–37], and potential applications[38–40]. As in the case of spatial optical vortices, the

Received: 15 November 2025
Accepted: 6 March 2026
Published online: 25 March 2026

[1]Key Laboratory of Light Field Manipulation and Information Acquisition, Ministry of Industry and Information Technology, School of Physical Science and Technology, Northwestern Polytechnical University, Xi'an 710129, China; [2]Nanophotonics Research Center, Institute of Microscale Optoelectronics & State Key Laboratory of Radio Frequency Heterogeneous, Shenzhen University, Shenzhen 518060, China; [3]School of Physics and Optoelectronic Engineering, Shandong University of Technology, Zibo 255000, China.
*Correspondence: YQ Zhang, E-mail: yqzhang@szu.edu.cn; T Mei, E-mail: ting.mei@ieee.org

spatiotemporal radius of STOV pulses exhibits a strong dependence on the topological charge[20,23], thereby limiting their applicability in scenarios that require the superposition of multiple vortices with different topological charges. To overcome this limitation, Ponomarenko et al. proposed the concept of perfect spatiotemporal optical vortices (PSTOVs) in 2014[41]. Unlike conventional STOVs, the radius of PSTOV pulses is independent of the topological charge. By employing spatiotemporal complex-amplitude modulation techniques, PSTOV pulses have recently been demonstrated experimentally[42,43]. However, these approaches require simultaneous control of both the amplitude and phase of the input pulse, which inevitably results in pronounced zeroth-order diffraction, especially for large topological charges. Moreover, current studies of PSTOVs are largely limited to the simplest annular intensity profiles. Achieving flexible control over the spatiotemporal distribution of PSTOVs would be of great interest for both fundamental studies and practical applications.

In this work, we report the experimental generation of a new class of PSTOV pulses with controllable polygonal shapes, which we refer to as generalized perfect spatiotemporal optical vortices (GPSTOVs). Unlike previous approaches, the generation of GPSTOV pulses relies on a pure-phase modulation strategy. The basic principle of our method is to encode a shape-controllable digital axicon together with a vortex phase in the spatiotemporal frequency domain. By introducing an azimuthal modulation to the axicon parameter, the intensity profiles of the generated GPSTOVs can be flexibly tailored while preserving their intrinsic "perfect" properties. Since amplitude modulation is not required, the proposed method achieves higher modulation efficiency and improved energy utilization. Experimental measurements show that the efficiency of our method is approximately 2.5 times that of conventional complex-amplitude modulation techniques. In addition to carrying transverse OAM, GPSTOV pulses provide an extra degree of freedom through their controllable geometric shapes, thereby holding promise for applications in diverse physical systems.

## 2 Results and discussion

### 2.1 Theoretical framework and numerical simulations

To provide deeper insight into the generation of polygonal GPSTOV pulses, we first briefly review the formation mechanism of PSTOVs with canonical annular shapes. Analogous to perfect spatial optical vortices[44], PSTOV pulses can be generated via the Fourier transform of a Bessel-Gaussian (BG) beam in the spatiotemporal frequency domain[42]:

$$\tilde{\psi}(r,\varphi) = J_\ell(\beta r)\exp\left(-\frac{r^2}{w_0^2}\right)\exp(\mathrm{i}\ell\varphi)\,, \qquad (1)$$

where $r = \sqrt{(k_x/\Delta k_x)^2 + (\Omega/\Delta\omega)^2}$ and $\varphi = \tan^{-1}(\Delta\omega k_x/\Delta k_x\Omega)$ are the normalized polar coordinates in the $k_x - \Omega$ plane. Here, $k_x$ denotes the spatial frequency along the $x$-direction, and $\Omega = \omega - \omega_0$ represents the temporal frequency defined relative to the central frequency $\omega_0$. $J_\ell$ is the $\ell$th-order Bessel function of the first kind, $w_0$ is the beam waist, and $\beta$ is a parameter that controls the radial profile of the BG mode. By performing a two-dimensional Fourier transform, we obtain the field distribution in the spatiotemporal domain (see detailed derivation in Supplementary Section 1):

$$\psi(\rho,\phi) = \int_0^{2\pi}\int_0^{\infty}\tilde{\psi}(r,\varphi)\exp[\mathrm{i}\rho r\cos(\varphi-\phi)]\;r\,\mathrm{d}r\mathrm{d}\varphi \propto \exp\left(-\frac{\rho^2+\beta^2}{w_1^2}\right)I_\ell\left(\frac{2\rho\beta}{w_1^2}\right)\exp(\mathrm{i}\ell\phi)\,, \qquad (2)$$

where $w_1 = 2/w_0$; $\rho = \sqrt{(x/\Delta x)^2 + (t/\Delta t)^2}$ and $\phi = \tan^{-1}(\Delta t x/\Delta x t)$ are the normalized polar coordinates in the $x - t$ plane. $I_\ell$ is the $\ell$th-order modified Bessel function of the first kind. Owing to its mathematical equivalence to the expression for perfect spatial optical vortices[45,46], Eq. (2) provides a valid description of the complex envelope of a PSTOV pulse. In the limit $\beta \gg w_1$, Eq. (2) can be further reduced to

$$\psi(\rho,\phi) \sim \exp\left[-\frac{(\rho-\beta)^2}{w_1^2}\right]\exp(\mathrm{i}\ell\phi)\,. \qquad (3)$$

It is evident that the intensity distribution of the field in Eq. (3) is independent of the topological charge $\ell$, which distinguishes PSTOVs from conventional STOVs. As demonstrated above, the key to synthesizing PSTOV pulses lies in the generation of a BG beam in the $k_x - \Omega$ domain. This can be achieved in two ways. One option is to directly generate the BG field [as given in Eq. (1)] using complex-amplitude modulation. The other is to encode a digital axicon together with a vortex phase. Both approaches yield similar results, but the latter offers higher efficiency due to pure-phase modulation.

We now showcase how to generate GPSTOV pulses with controllable polygonal shapes via pure-phase modulation in a 4f pulse shaper. The conceptual illustration is shown in Fig. 1(a). Starting with a generic Gaussian pulsed beam, its spectrum is first dispersed by a grating and subsequently collimated by a cylindrical lens before being incident on a spatial light modulator (SLM). With such a configuration, the location of the SLM can be regarded as the $k_x - \Omega$ plane. To synthesize polygonal GPSTOV pulses, the SLM is encoded with a phase hologram given by:

$$\phi_{\mathrm{SLM}}(r,\varphi) = \mathrm{mod}\{2\pi\alpha f(\varphi)\,r + \ell\varphi, 2\pi\}\,, \qquad (4)$$

with

$$f(\varphi) = 1 - \frac{1}{p}\sin(q\varphi)\;\;, \qquad (5)$$

here, $(r,\varphi)$ are the normalized polar coordinates in the $k_x - \Omega$ plane. Equation (4) can be interpreted as the superposition of a shape-controllable digital axicon and a vortex

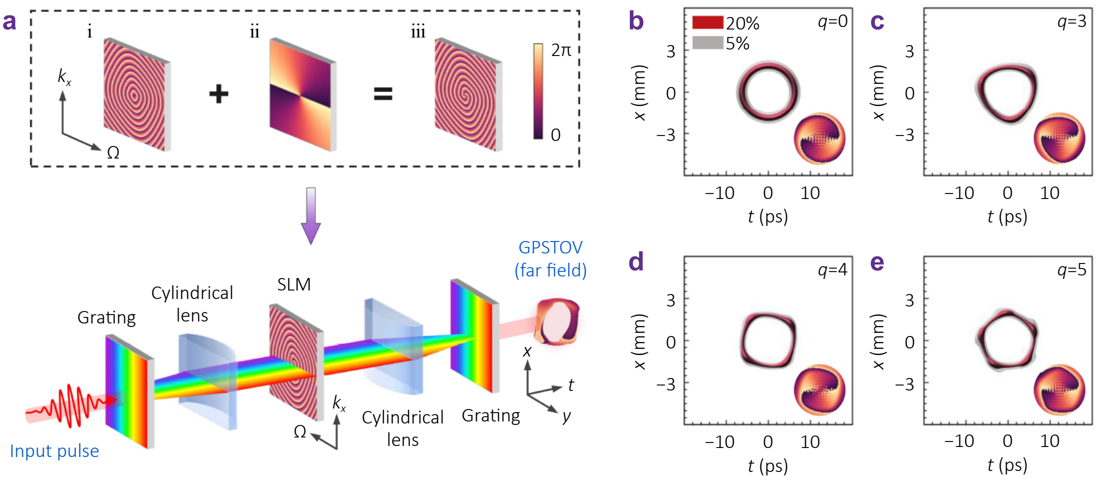


Fig. 1 | Principle of GPSTOV pulse generation. (a) Conceptual illustration of GPSTOV pulse generation via pure-phase modulation in a 4f pulse shaper. The phase hologram encoded on the spatial light modulator (SLM) is obtained by superposing a shape-controllable digital axicon (i) with a vortex phase (ii). (b–e) Simulated spatiotemporal distributions of GPSTOV pulses with various shapes, calculated using Eq. (6). The parameters are set as $\omega_0$=2.36×10$^{15}$ rad/s ($\lambda_0$=800 nm), $\Delta\omega$=4×10$^{12}$ rad/s, $\Delta k_x$=13.333 rad/mm, and $\alpha$=4, consistent with the experimental conditions.

phase with topological charge $\ell$. As shown in Supplementary Section 2, the spatiotemporal radius of PSTOV pulses scales linearly with the axicon parameter $\alpha$. The function $f(\varphi)$ modulates $\alpha$ along the azimuthal direction, thereby inducing a corresponding azimuthal variation in the spatiotemporal radius. This mechanism provides the physical basis for the generation of polygonal GPSTOV pulses (Supplementary Section 3). As indicated by Eq. (5), the geometric structure of GPSTOV pulses is governed by two dimensionless parameters, where $p$ and $q$ control the curvature and symmetry-order of the field, respectively. Accordingly, triangular, square, and pentagonal GPSTOV pulses can be generated by setting $q=3$, 4, and 5, respectively. In the special case $q=0$ (or equivalently, $f(\varphi)=1$), the polygonal GPSTOV pulses transform into regular PSTOV pulses with annular profiles, as depicted in Fig. 1(b–e).

At the far field (i.e., the spatial Fourier plane) of the 4f pulse shaper, the resulting spatiotemporal field can be calculated as:

$$\psi(x,t)=\iint \tilde{\psi}_G(k_x,\Omega)\exp\left[\mathrm{i}\phi_{\mathrm{SLM}}(k_x,\Omega)\right] \cdot \exp\left[\mathrm{i}(k_x x-\Omega t)\right]\mathrm{d}k_x\mathrm{d}\Omega\ , \tag{6}$$

where $\widetilde{\psi}_G(k_x,\Omega)=\exp\left[-(k_x/\Delta k_x)^2-(\Omega/\Delta\omega)^2\right]$ represents the Fourier spectrum of the input pulse, and $\phi_{\mathrm{SLM}}(k_x,\Omega)$ is the phase pattern encoded on the SLM. For a transform-limited Gaussian pulse, its spatial and temporal bandwidths can be determined by $\Delta k_x=2/\Delta x$ and $\Delta\omega=2/\Delta t$, where $\Delta x$ and $\Delta t$ denote the pulse widths in the $x$- and $t$-directions, respectively.

## 2.2 Experimental setup

The system for generating and characterizing the GPSTOV pulses is illustrated in Fig. 2. Femtosecond pulses (~120 fs) from a Ti:sapphire amplifier, centered at ~800 nm, are first split into a signal pulse and a reference pulse by a beam splitter (BS1). The signal pulse is then directed into a custom 4f pulse shaper consisting of a diffraction grating (1200 lines/mm), a cylindrical lens (CL1, $f$ = 300 mm along the $y$-axis), and a reflective spatial light modulator (SLM; X15213-02, Hamamatsu). The SLM is positioned at the focal plane of CL1 and is programmed with a phase hologram $\phi_{\mathrm{SLM}}$ [Eq. (4)], enabling modulation of the signal pulse in the $k_x-\Omega$ domain. An adjustable slit placed before the SLM is used to tailor the temporal bandwidth. After phase modulation, the spatially dispersed spectral components are reflected back and recombined at the grating. This process can be understood as a temporal Fourier transform ($\Omega\rightarrow t$). Finally, the output pulse from the pulse shaper is spatially Fourier-transformed by a second cylindrical lens (CL2, $f$ = 850 mm along the $x$-axis). At the focal plane (defined as $z=0$), a GPSTOV pulse with controllable geometric shapes is generated.

The characterization of the generated GPSTOV pulses is performed using a three-dimensional (3D) diagnostic technique implemented in a Mach-Zehnder interferometer[23,47]. The reference path includes a high-precision translation stage (Delay Line, N-565, PI), which allows the relative time delay between the GPSTOV pulse and the reference pulse to be precisely controlled. When the two pulses overlap in space and time, interference fringes are produced and recorded by a CCD camera (BFLY-U3-23S6C-C, Point Grey). Owing to its considerably shorter duration, the reference pulse interferes with each temporal slice of the GPSTOV pulse as it is scanned along the time axis. Consequently, the full 3D spatiotemporal profile of the generated GPSTOV pulse can be reconstructed form the delay-dependent interference patterns (see Supplementary Section 5).

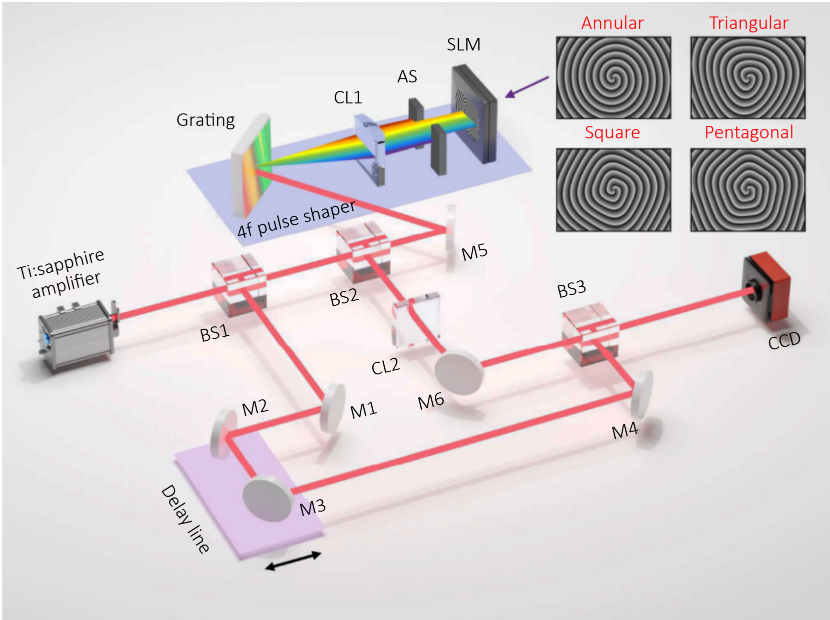


Fig. 2 | Experimental setup for the generation and characterization of GPSTOV pulses. Insets: phase holograms encoded on the SLM. (BS, beam splitter; M, mirror; CL, cylindrical lens; AS, adjustable slit; SLM, spatial light modulator; CCD, charge-coupled-device.)

## 2.3 Generation of annular PSTOV pulses

As discussed previously, by setting the parameter $q=0$ [Eq. (5)], regular PSTOV pulses with canonical annular profiles can be obtained. To verify our theoretical predictions, we first experimetally observed the intensity and phase distributions of PSTOV pulses with typical topological charges $\ell=2,\ 4,\ 6,$ and 8 [Fig. 3(a–d)]. In the experiments, the axicon parameter $\alpha$ was fixed at 4. A larger value of $\alpha$ leads to an increased PSTOV radius (Supplementary Section 2); however, it also requires a detector with a larger aperture. Despite slight distortions, the experimental results show good agreement with the simulated results presented in Fig. S1. The observed non-uniform intensity distributions can be attributed to a small misalignment between the beam center and the phase hologram on the SLM (see Supplementary Section 6 for details). The white circles in the phase distributions highlight the helical phase structures in the $x-t$ plane.

To further evaluate the "perfect" characteristics of the generated PSTOV, we measured the radius variations of different topological charges in both the spatial and temporal dimensions, as plotted in Fig. 3(e) and 3(f). For comparison, the corresponding simulated results are also included. It can be observed that the beam radius is not completely intendent of the topological charge, although this dependence is not strikingly apparent when considering topological charges in a limited range (e.g., $\ell<10$). This behavior arises because an ideal PSTOV corresponds to the Fourier transform of a Bessel beam, which cannot be experimentally realized due to its infinite energy. Given the linear correlation between the beam radius and the axicon parameter $\alpha$, the slight radius variation can be effectively compensated, if desired, by adjusting $\alpha$ for each value of $\ell$.

## 2.4 Generation of GPSTOV pulses with polygonal shapes

The function $f(\varphi)$ introduces a modulation to the local gradient of the spectral phase. The resulting non-uniform phase gradient redistributes the energy in the spatiotemporal domain, leading to the formation of localized intensity maxima ("hot spots") at the vertices of the polygonal GPSTOV pulses, as shown in Fig. 4. To quantitatively assess the quality of the generated field, we define a uniformity parameter as follows:

$$U=1-\frac{\max(I)-\min(I)}{\max(I)+\min(I)}. \tag{7}$$

The uniformity $U$ characterizes the intensity fluctuations along the polygonal profiles. Clearly, the uniformity depends on both parameters $p$ and $q$. For a fixed value of $q$, the uniformity increases with increasing $p$. However, when $p$ increases infinitely, $f(\varphi)\to 1$, and the polygonal profile gradually approaches an annular distribution. In contrast, for a fixed value of $p$, the uniformity decreases as $q$ increases. Therefore, when $q$ is increased, $p$ must be increased accordingly to maintain a high uniformity (see more details in Supplementary Section 4).

By selecting appropriate parameter combinations based on the uniformity criterion ($U\approx 0.5$), we experimentally generated GPSTOV pulses with triangular ($q=3, p=15$), square ($q=4, p=20$), and pentagonal ($q=5, p=25$) shapes under different topological charges, as shown in

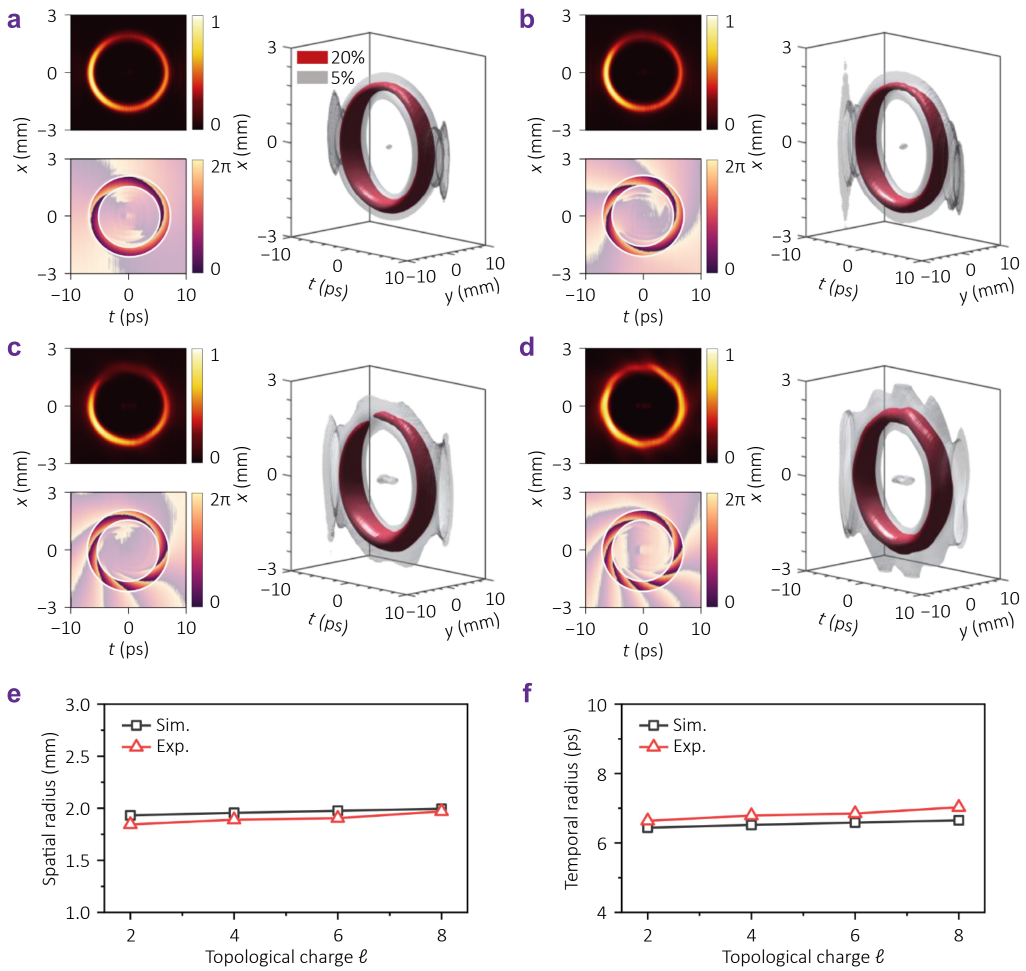


Fig. 3 | Generation of PSTOV pulses with annular profiles. (a–d) Experimental results of annular PSTOV pulses with topological charges ℓ = 2, 4, 6 and 8, respectively. The results in each panel include the intensity distribution in the *x*-*t* plane (top left), the phase distribution in the *x*-*t* plane (bottom left), and the 3D iso-intensity profile (right). (e, f) Dependence of the spatial and temporal radii on the topological charge ℓ. (Sim.: simulated results; Exp.: experimental results.)

Fig. 5(a) and 5(b). Benefiting from the high energy utilization of pure-phase modulation, our method achieves an efficiency exceeding 90% for these typical GPSTOV pulses, which is nearly 2.5 times that of conventional complex-amplitude modulation techniques (see Supplementary Section 7 for details). Furthermore, by comparing the intensity distributions for $\ell=2$ and $\ell=6$, we find that the polygonal GPSTOV pulses exhibit similar "perfect" characteristics to the PSTOV pulses with annular profiles (Fig. 3). As illustrated in Fig. 5(c) and 5(d), the spatial and temporal widths of the GPSTOV pulses remain nearly unchanged as the topological charge increases from 2 to 6. All the above experimental observations agree well with the numerical simulations shown in Fig. S10, as further verified by the correlation coefficients summarized in Table S1 (see Supplementary Section 8 for details).

The reconstructed 3D iso-intensity profiles, together with the corresponding simulated results, are shown in Fig. 6. Due to the limited fill factor (96.8%) of the SLM, a small portion of the input pulse remains unmodulated, giving rise to a zeroth-order diffraction spot at the center of the generated GPSTOV pulses. Compared with the outer polygonal contours, these zeroth-order spots are sufficiently weak. For a quantitative assessment, we calculated the energy ratio (i.e., the ratio of the integrated intensity) between the zeroth-order component and the desired GPSTOV pulse. In our measurements, the maximum energy ratio is evaluated to be ~2.41%, which can be neglected for most laser applications. If necessary, the residual zeroth-order component can be removed by applying a phase grating in the $k_x-\Omega$ domain; however, this approach would introduce additional diffraction orders and result in further energy loss.

## 3 Conclusions

In conclusion, we have proposed a pure-phase modulation strategy for generating generalized perfect spatiotemporal optical vortices (GPSTOVs). As a new class of PSTOVs,

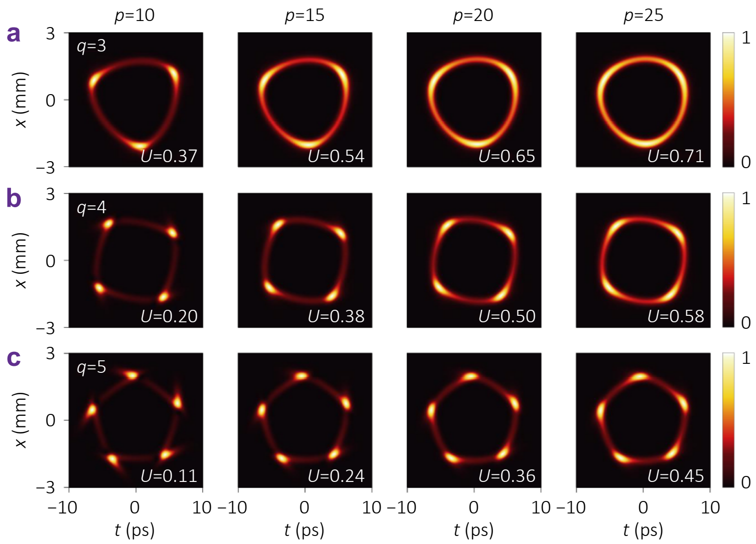


Fig. 4 | Simulated distributions of polygonal GPSTOV pulses for different parameters. (a) $q$ = 3. (b) $q$ = 4. (c) $q$ = 5. From left to right, the four columns correspond to distributions with $p$ = 10, $p$ = 15, $p$ = 20, and $p$ = 25, respectively. The corresponding uniformity values are given in the lower-right corner of each figure.

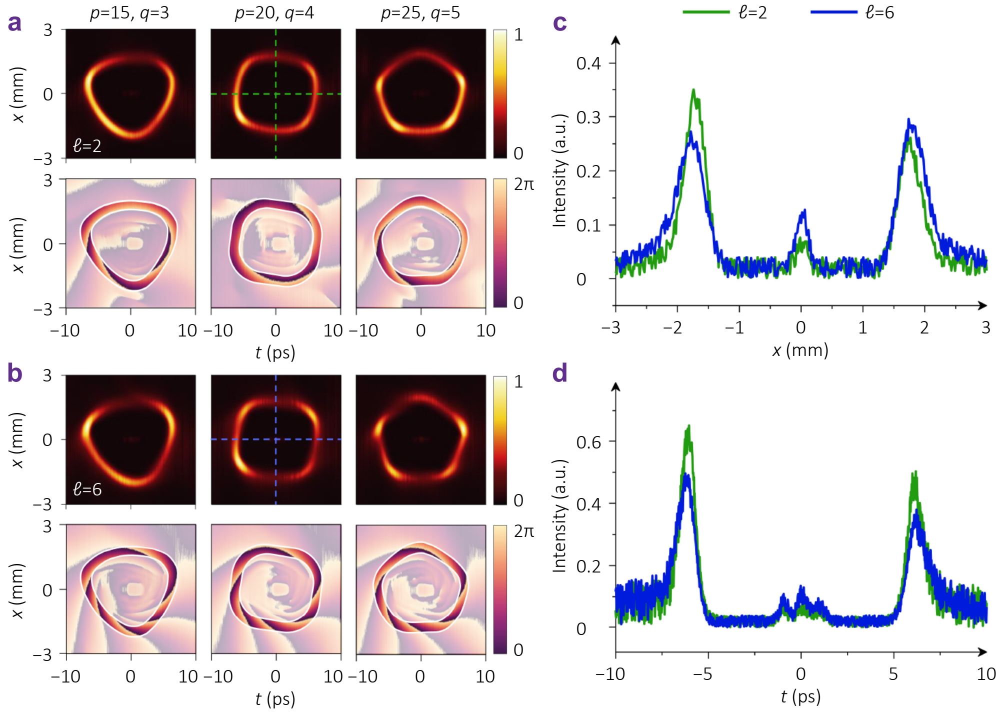


Fig. 5 | Generation of GPSTOV pulses with polygonal shapes. (a) Experimental results of triangular, square, and pentagonal GPSTOV pulses with a topological charge of $\ell$ = 2. The upper and lower panels show the spatiotemporal intensity and phase distributions in the $x$-$t$ plane, respectively. (b) Same as (a), but with a topological charge of $\ell$ = 6. (c, d) Comparison of the one-dimensional (1D) intensity profiles extracted along the dotted lines indicated in (a, b), respectively.

GPSTOV pulses possess simultaneously two remarkable features: topological-charge-independent spatiotemporal sizes and fully controllable geometric shapes. By precisely tuning the phase parameters in the spatiotemporal frequency domain, we achieved high-efficiency generation of both PSTOV pulses with annular profiles and GPSTOV pulses with polygonal shapes. The measured modulation efficiency exceeds 90%, which cannot be attained using

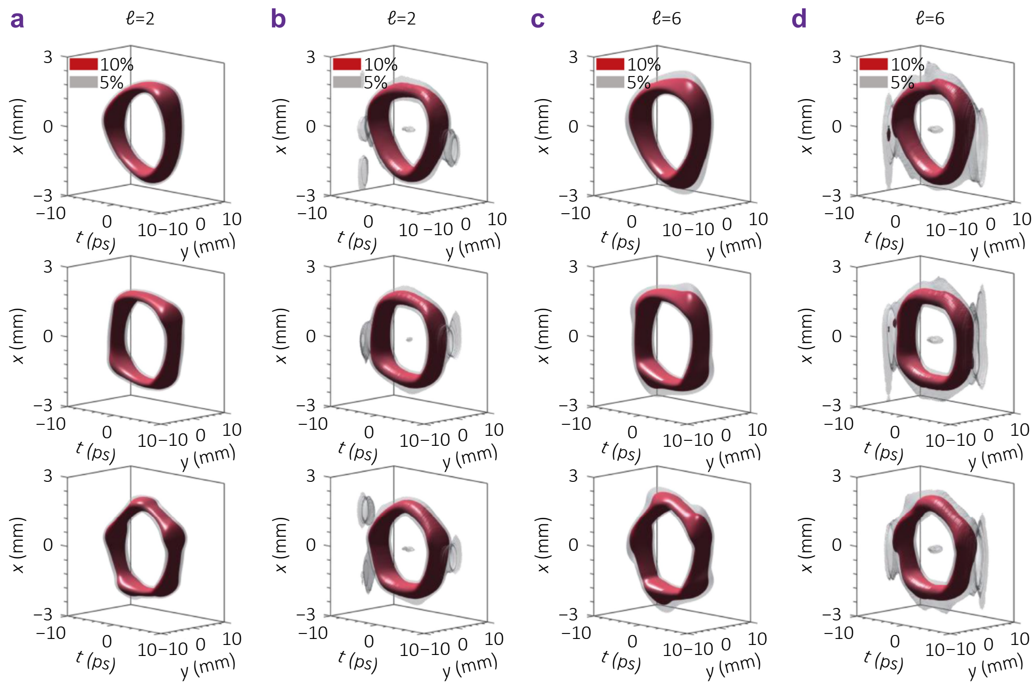


Fig. 6 | 3D distributions of polygonal GPSTOV pulses. (a) Numerically simulated 3D iso-intensity profiles of polygonal GPSTOV pulses with a topological charge of $\ell$ = 2. (b) Experimentally reconstructed 3D iso-intensity profiles corresponding to (a). (c, d) Same as (a, b), but with a topological charge of $\ell$ = 6.

complex-amplitude modulation techniques. In addition to typical polygonal structures, our method also allows the generation of GPSTOV pulses with more complex configurations (see Supplementary Section 9 for details).

Beyond their conceptual novelty, the unique features of GPSTOV pulses may open up a wide range of potential applications. Analogous to spatial optical vortices carrying longitudinal OAM, STOVs with transverse OAM could serve as carriers for information encoding and transmission[48,49]. However, due to the imbalance between diffraction and dispersion effects, conventional STOVs cannot propagate stably in free space[18,35]. This instability not only limits long-distance transmission but also increases the bit-error rate during information transfer. In contrast, the GPSTOV pulses exhibit significantly enhanced propagation stability (see Supplementary Section 10 for details), making them more attractive for optical communication applications. Moreover, the programmable geometric profiles of GPSTOV pulses provide an additional degree of freedom for information encoding. For example, different polygonal shapes could function as distinct communication channels, thereby increasing the information capacity of communication systems. GPSTOV pulses may also enable new possibilities in optical trapping and particle manipulation. Under the excitation of high-intensity femtosecond pulses, many particles, particularly metallic ones, exhibit pronounced nonlinear responses[50,51]. In such nonlinear regimes, the dynamical behavior of particles is strongly governed by the spatiotemporal characteristics of the excitation light field[52,53]. Therefore, integrating spatiotemporally coupled GPSTOV pulses with nonlinear optical tweezer systems may reveal previously unexplored trapping phenomena.

Overall, although the potential applications of GPSTOV pulses are promising, further studies are still required to fully understand the physical properties of these spatiotemporal wavepackets. With continued exploration, it is anticipated that a broader range of applications will emerge in the near future.

## References

1. Bliokh KY, Nori F. Transverse and longitudinal angular momenta of light. *Phys Rep* **592**, 1–38 (2015).
2. Allen L, Beijersbergen MW, Spreeuw RJC et al. Orbital angular momentum of light and the transformation of Laguerre-Gaussian laser modes. *Phys Rev A* **45**, 8185 (1992).
3. Shen YJ, Wang XJ, Xie ZW et al. Optical vortices 30 years on: OAM manipulation from topological charge to multiple singularities. *Light Sci Appl* **8**, 90 (2019).
4. Pu MB, Li X, Ma XL et al. Catenary optics for achromatic generation of perfect optical angular momentum. *Sci Adv* **1**, e1500396 (2015).
5. Guo YH, Pu MB, Zhao ZY et al. Merging geometric phase and plasmon retardation phase in continuously shaped metasurfaces for arbitrary orbital angular momentum generation. *ACS Photonics* **3**, 2022–2029 (2016).
6. Guo YH, Zhang SC, Pu MB et al. Spin-decoupled metasurface for simultaneous detection of spin and orbital angular momenta via momentum transformation. *Light Sci Appl* **10**, 63 (2021).
7. Zhang Z, Li GY, Liu YL et al. Robust measurement of orbital angular momentum of a partially coherent vortex beam under amplitude and

phase perturbations. *Opto-Electron Sci* **3**, 240001 (2024).

8. Padgett M, Bowman R. Tweezers with a twist. *Nat Photonics* **5**, 343–348 (2011).
9. Yang YJ, Ren YX, Chen MZ et al. Optical trapping with structured light: a review. *Adv Photonics* **3**, 034001 (2021).
10. Willner AE, Huang H, Yan Y et al. Optical communications using orbital angular momentum beams. *Adv Opt Photonics* **7**, 66–106 (2015).
11. Wang J, Liu J, Li SH et al. Orbital angular momentum and beyond in free-space optical communications. *Nanophotonics* **11**, 645–680 (2022).
12. Kozawa Y, Matsunaga D, Sato S. Superresolution imaging via superoscillation focusing of a radially polarized beam. *Optica* **5**, 86–92 (2018).
13. Fickler R, Lapkiewicz R, Plick WN et al. Quantum entanglement of high angular momenta. *Science* **338**, 640–643 (2012).
14. Nape I, Sephton B, Ornelas P et al. Quantum structured light in high dimensions. *APL Photonics* **8**, 051101 (2023).
15. Chen W, Liu Y, Lu YQ. Spatiotemporal optical vortices: toward tailoring orbital angular momentum of light in full space-time. *ACS Photonics* **10**, 2011–2019 (2023).
16. Wan CH, Chong A, Zhan QW. Optical spatiotemporal vortices. *eLight* **3**, 11 (2023).
17. Jhajj N, Larkin I, Rosenthal EW et al. Spatiotemporal optical vortices. *Phys Rev X* **6**, 031037 (2016).
18. Hancock SW, Zahedpour S, Goffin A et al. Free-space propagation of spatiotemporal optical vortices. *Optica* **6**, 1547–1553 (2019).
19. Chong A, Wan CH, Chen J et al. Generation of spatiotemporal optical vortices with controllable transverse orbital angular momentum. *Nat Photonics* **14**, 350–354 (2020).
20. Cao Q, Chen J, Lu KY et al. Non-spreading Bessel spatiotemporal optical vortices. *Sci Bull* **67**, 133–140 (2022).
21. Chen W, Zhang W, Liu Y et al. Time diffraction-free transverse orbital angular momentum beams. *Nat Commun* **13**, 4021 (2022).
22. Huang JY, Zhang JH, Zhu TF et al. Spatiotemporal differentiators generating optical vortices with transverse orbital angular momentum and detecting sharp change of pulse envelope. *Laser Photonics Rev* **16**, 2100357 (2022).
23. Liu X, Cao Q, Zhang NJ et al. Spatiotemporal optical vortices with controllable radial and azimuthal quantum numbers. *Nat Commun* **15**, 5435 (2024).
24. Huo PC, Chen W, Zhang ZX et al. Observation of spatiotemporal optical vortices enabled by symmetry-breaking slanted nanograting. *Nat Commun* **15**, 3055 (2024).
25. Ni XQ, Liu Y, Lou BC et al. Three-dimensional reconfigurable optical singularities in bilayer photonic crystals. *Phys Rev Lett* **132**, 073804 (2024).
26. Ye JY, Che ZY, Wang JJ et al. Propagation-invariant spatiotemporal vortices. *Sci Bull* **70**, 3758–3763 (2025).
27. Chen J, Lu KY, Cao Q et al. Automated close-loop system for three-dimensional characterization of spatiotemporal optical vortex. *Front Phys* **9**, 633922 (2021).
28. Gui G, Brooks NJ, Wang B et al. Single-frame characterization of ultrafast pulses with spatiotemporal orbital angular momentum. *ACS Photonics* **9**, 2802–2808 (2022).
29. Hancock SW, Zahedpour S, Milchberg HM. Transient-grating single-shot supercontinuum spectral interferometry (TG-SSSI). *Opt Lett* **46**, 1013–1016 (2021).
30. Hancock S, Zahedpour S, Milchberg H. Mode structure and orbital angular momentum of spatiotemporal optical vortex pulses. *Phys Rev Lett* **127**, 193901 (2021).
31. Hancock SW, Zahedpour S, Milchberg HM. Second-harmonic generation of spatiotemporal optical vortices and conservation of orbital angular momentum. *Optica* **8**, 594–597 (2021).
32. Gui G, Brooks NJ, Kapteyn HC et al. Second-harmonic generation and the conservation of spatiotemporal orbital angular momentum of light. *Nat Photonics* **15**, 608–613 (2021).
33. Mazanov M, Sugic D, Alonso MA et al. Transverse shifts and time delays of spatiotemporal vortex pulses reflected and refracted at a planar interface. *Nanophotonics* **11**, 737–744 (2022).
34. Huang SL, Wang P, Shen X et al. Diffraction properties of light with transverse orbital angular momentum. *Optica* **9**, 469–472 (2022).
35. Porras MA. Propagation of higher-order spatiotemporal vortices. *Opt Lett* **48**, 367–370 (2023).
36. Cao Q, Chen Z, Zhang C et al. Propagation of transverse photonic orbital angular momentum through few-mode fiber. *Adv Photonics* **5**, 036002 (2023).
37. Martín-Hernández R, Gui G, Plaja L et al. Extreme-ultraviolet spatiotemporal vortices via high harmonic generation. *Nat Photonics* **19**, 817–824 (2025).
38. Huang SL, Li ZW, Li JW et al. Spatiotemporal vortex strings. *Sci Adv* **10**, eadn6206 (2024).
39. Dong JH, Xu L, Fang YQ et al. Scheme for generation of spatiotemporal optical vortex attosecond pulse trains. *Photonics Res* **12**, 2409–2417 (2024).
40. Teng HA, Liu X, Zhang NJ et al. Construction of optical spatiotemporal skyrmions. *Light Sci Appl* **14**, 324 (2025).
41. Ponomarenko SA, Hebri D. Perfect space-time vortices. *Opt Lett* **49**, 4322–4325 (2024).
42. Fan HH, Cao Q, Liu X et al. Perfect spatiotemporal optical vortices. *Photonics Res* **13**, 1776–1782 (2025).
43. Cheng J, Wu ZL, Sun A et al. Spatiotemporal optical vortices with invariant radius and width. *Laser Photonics Rev* **19**, e00318 (2025).
44. Liu XJ, Gu MN, Tian Y et al. Research progress on generating perfect vortex beams based on metasurfaces. *Opto-Electron Sci* **4**, 250007 (2025).
45. Vaity P, Rusch L. Perfect vortex beam: Fourier transformation of a Bessel beam. *Opt Lett* **40**, 597–600 (2015).
46. Pinnell J, Rodríguez-Fajardo V, Forbes A. How perfect are perfect vortex beams?. *Opt Lett* **44**, 5614–5617 (2019).
47. Li H, Bazarov IV, Dunham BM et al. Three-dimensional laser pulse intensity diagnostic for photoinjectors. *Phys Rev ST Accel Beams* **14**, 112802 (2011).
48. Wu ZL, Cheng J, Wan CH. Optical data encoding through spatiotemporal orbital angular momentum spectral engineering. *ACS Photonics* **12**, 5017–5023 (2025).
49. Feng F, Hou GZ, Zhang ZY et al. Spatiotemporal optical vortex combs. *Nat Commun* **16**, 11652 (2025).
50. Jiang YQ, Narushima T, Okamoto H. Nonlinear optical effects in trapping nanoparticles with femtosecond pulses. *Nat Phys* **6**, 1005–1009 (2010).
51. Zhang YQ, Shen JF, Min CJ et al. Nonlinearity-induced multiplexed optical trapping and manipulation with femtosecond vector beams. *Nano Lett* **18**, 5538–5543 (2018).
52. Qin YQ, Zhou LM, Huang L et al. Nonlinearity-induced nanoparticle circumgyration at sub-diffraction scale. *Nat Commun* **12**, 3722 (2021).
53. Zhu Z, Zhang YQ, Zhang SS et al. Nonlinear optical trapping effect with reverse saturable absorption. *Adv Photonics* **5**, 046006 (2023).

## Acknowledgements

This work was supported by the Guangdong Basic and Applied Basic Research Foundation (2026B1515020039), the National Natural Science Foundation of China (62375177, 12174310, 62575184, 12474294, and 12534017), Shenzhen Science and Technology Program (RCJC20210609103232046), Project of DEGP (2024ZDZX2019), Taishan Scholars Program of Shandong Province (tsqn202507178), Research Team Cultivation Program of Shenzhen University (2023QNT014), and Shenzhen University 2035 Initiative ( 2023B004).

## Author contributions

S.S.Z. conducted the numerical simulations. S.S.Z. and Z.Y.Z. built the experimental configuration and performed experimental measurements. Q.Y.W. assisted with the data processing. S.S.Z. prepared the initial draft of the manuscript. Z.S.M., W.D.Z., C.J.M., and X.C.Y. reviewed the manuscript and contributed to the final version. T.M. and Y.Q.Z. supervised the overall work. All authors discussed the results and commented on the manuscript.

## Competing interests

The authors declare no competing financial interests.

## Supplementary information

Supplementary information for this paper is available at https://doi.org/10.29026/oes.2026.250041


Published by Editorial Office of *Opto-Electronic Science*, Institute of Optics and Electronics, Chinese Academy of Sciences.